J Mater Sci (2010) 45:2442–2448
DOI 10.1007/s10853-010-4215-z

Solvent-free synthesis of hexagonal barium ferrite ($BaFe_{12}O_{19}$) particles

Yunchen Du · Haibin Gao · Xinrong Liu · Jingyu Wang · Ping Xu · Xijiang Han

Received: 7 August 2009 / Accepted: 8 January 2010 / Published online: 20 January 2010

Abstract M-type barium ferrite ($BaFe_{12}O_{19}$) particles, from a mixture of barium nitrate, ferric nitrate, cetyltrimethylammonium bromide (CTAB), and ammonium carbonate, have been successfully prepared through simple grinding and calcination in the absence of any solvent. The products are characterized by X-ray diffraction, scanning electron microscope, and vibrating sample magnetometer, whose results indicate that they have well crystalline phase of $BaFe_{12}O_{19}$, typically hexagonal platelet-like structure, large saturation magnetization, even submicrometer particle size under the optimum condition. Meanwhile, the effects of Fe/Ba ratio, CTAB, and ammonium carbonate are also investigated. It has been found that the proper Fe/Ba ratio could suppress the intermediate phase such as α-Fe_2O_3 and $BaFe_2O_4$, CTAB could promote the crystallinity of $BaFe_{12}O_{19}$ and produce hexagonal crystal structure, and ammonium carbonate was the key for forming $BaFe_{12}O_{19}$ phase. This facile method may be helpful for the preparation of other multicomponent functional materials.

Introduction

M-type barium ferrite ($BaFe_{12}O_{19}$) with hexagonal crystal structure has received much attention due to its excellent chemical and physical properties such as large magnetocrystalline anisotropy, high Curie temperature, relatively large saturation magnetization and corrosion resistivity [1–3], which make it potentially important in high density perpendicular recording media, magnetic fluids, certain microwave devices, etc. [4–7]. Conventional ceramic method from iron oxides and barium carbonate requires quite high-calcination temperature (>1200 °C), and always leads to sintering and aggregation on the particles [8]. Although ball milling can decrease the particle size and improve its magnetic properties effectively, it brings some unexpected disadvantages such as damaged hexagonal configuration, impurities, and lattice strains [9].

In the past decades, many potential methods have been used to prepare homogeneous fine barium ferrite ($BaFe_{12}O_{19}$) particles, including coprecipitation [10–12], hydrothermal or microwave hydrothermal synthesis [3, 13–15], ammonium nitrate melt technique [16, 17], sol–gel method [18–22], microemulsion [23, 24], glass crystallization method [25], sugar-nitrates process [26], etc. As expected, most of the products exhibit much smaller particle sizes than that from conventional ceramic method, which results in their characteristics of single magnetic domains. However, compared with conventional ceramic method, a gap to real industrial applications still exists as these routes always possess relatively complex preparative process and rigorous conditions, even a large amount of waste alkaline solution. Therefore, it is still desirable to develop a facile, rapid and environmentally benign route for hexagonal barium ferrite with small particle size.

Recently, many scientists have shown their interests in preparing various functional materials through solvent-free route [27–36]. Following this direction, we demonstrated here a quite simple method to synthesize barium ferrite ($BaFe_{12}O_{19}$) through grinding and calcining a solid-state mixture (barium nitrate, ferric nitrate, CTAB, and ammonium carbonate). Very interestingly, the obtained products

Y. Du (✉) · H. Gao · X. Liu · J. Wang · P. Xu · X. Han (✉)
Chemistry Laboratory Center, Department of Chemistry, Harbin Institute of Technology, Harbin 150001, China
e-mail: yunchendu@yahoo.com.cn

X. Han
e-mail: hanxj63@yahoo.com.cn

exhibit well crystalline phase of $BaFe_{12}O_{19}$, typically hexagonal platelet-like structure, large saturation magnetization, and submicrometer particle size under the optimum condition. On the other hand, the effects of Fe/Ba ratio, CTAB, and ammonium carbonate amounts in this route are also investigated.

Experimental section

Sample preparation

In a typical synthesis of $BaFe_{12}O_{19}$ particles, required amounts of cetyltrimethylammonium bromide (CTAB), ferric nitrate [$Fe(NO_3)_3 \cdot 9H_2O$], and barium nitrate [$Ba(NO_3)_2$] were ground in an agate mortar for 15 min at room temperature. Then, ammonium carbonate [$(NH_4)_2CO_3$)] was added, the mixture was ground for another 20 min. The obtained viscous solid was dried at 120 °C for 4 h, followed by precalcination at 400 °C for 4 h and calcination at 950 °C for 6 h. The corresponding designation and composition have been listed in Table 1.

Characterization

Powder X-ray diffraction (XRD) data were recorded on an XRD-6000 X-ray diffractometer (Shimadzu) with a Cu Kα radiation source (40.0 kV, 30.0 mA). Scanning electron microscope (SEM) images were obtained on the S-4800 (Hitachi) scanning microscope, and the samples were mounted on aluminum studs using adhesive graphite tape and sputtercoated with gold before analysis. The magnetic properties (intrinsic coercivity, saturation, and remanent magnetization) were measured using a vibrating sample magnetometer (VSM, Lake Shore7307).

Table 1 The designation and composition of prepared samples

Sample	$Fe(NO_3)_3 \cdot 9H_2O$ (g)	$Ba(NO_3)_2$ (g)	Fe/Ba ratio	CTAB (g)	$(NH_4)_2CO_3$ (g)
BF1	4.848	0.313	10	2.0	4.0
BF2	4.848	0.285	11	2.0	4.0
BF3	4.848	0.261	12	2.0	4.0
BF4	4.848	0.285	11	0	4.0
BF5	4.848	0.285	11	1.0	4.0
BF6	4.848	0.285	11	2.0	4.0
BF7	4.848	0.285	11	3.0	4.0
BF8	4.848	0.285	11	2.0	0
BF9	4.848	0.285	11	2.0	2.0
Bf10	4.848	0.285	11	2.0	4.0
BF11	4.848	0.285	11	2.0	6.0

BF2, BF6, and BF10 are identical samples, the different designation is convenient for discussion

Results and discussion

The effect of Fe/Ba ratio

It has been reported that Fe/Ba ratio played an important role in the synthesis of barium ferrite ($BaFe_{12}O_{19}$) [21, 37, 38]. Generally, a stoichiometric amount of barium will produce the intermediate phase α-Fe_2O_3 and too much barium will produce another intermediate $BaFe_2O_4$ phase, both of them can reduce the specific saturation magnetization of $BaFe_{12}O_{19}$. The optimum Fe/Ba ratio is strongly dependent on the preparation method and the starting materials [37, 38], thus, it may be primary to find an appropriate Fe/Ba ratio in the solvent-free route for minimizing α-Fe_2O_3 and $BaFe_2O_4$.

Figure 1 shows the XRD patterns of BF1, BF2, and BF3, which are synthesized under the same condition except different Fe/Ba ratio (Table 1). All samples exhibit typical peaks that can be indexed to the standard pattern of M-type $BaFe_{12}O_{19}$ crystals (JCPDS 27-1029), indicating that the solvent-free route is feasible for the formation of $BaFe_{12}O_{19}$. Similar to previous works [6, 18, 39, 40], there are also tiny impurities such as α-Fe_2O_3 and $BaFe_2O_4$, whose contents are obviously influenced by the Fe/Ba ratio. For example, when the Fe/Ba ratio is 12, there is a well-resolved peak at near 33.1° (Fig. 1c), so that α-Fe_2O_3 (JCPDS 24-0072) can be taken as the major impurity. When the Fe/Ba ratio is 11, the intensity of this peak becomes very weak, while tiny $BaFe_2O_4$ (JCPDS 25-1191) can be detected (about 28.4° in Fig. 1b). Further decreasing the Fe/Ba ratio to 10, this leads to the increasing content of

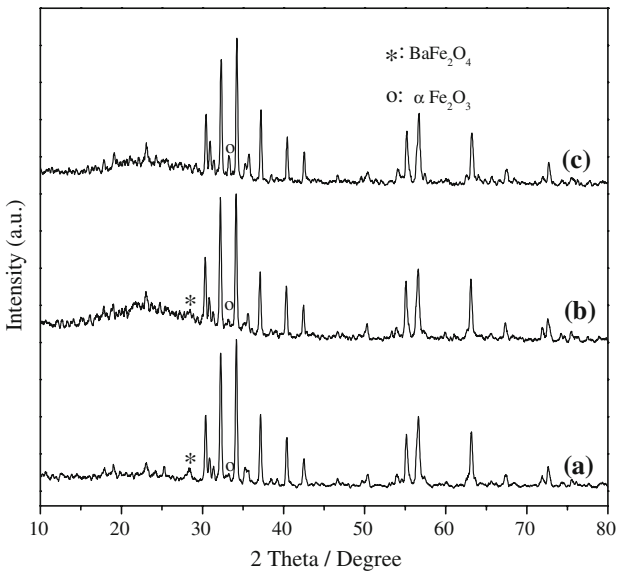

Fig. 1 XRD patterns of $BaFe_{12}O_{19}$ particles with different Fe/Ba ratio. BF1 (*a*), BF2 (*b*), and BF3 (*c*)

$BaFe_2O_4$ without eliminating the residual phase of α-Fe_2O_3 (Fig. 1a). Therefore, we reckon that the Fe/Ba ratio of 11 may be a better choice for high-purity $BaFe_{12}O_{19}$ in the current method.

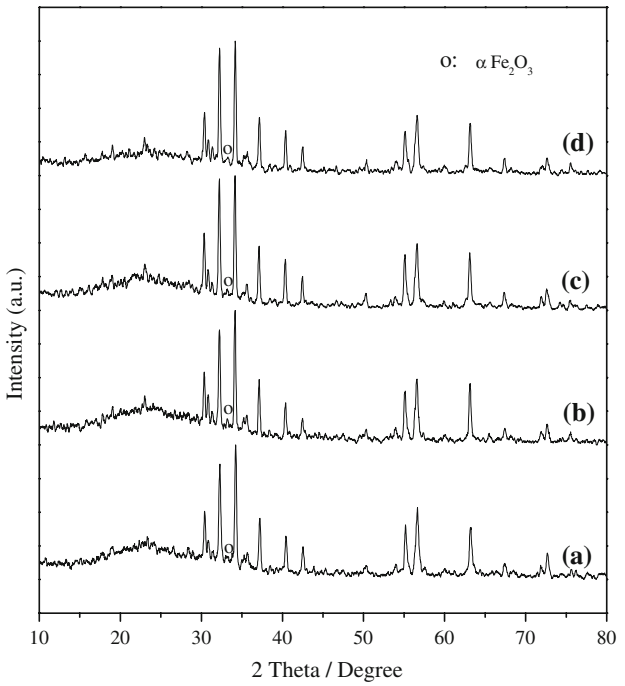

Fig. 2 XRD patterns of $BaFe_{12}O_{19}$ particles with different amount of CTAB. BF4 (*a*), BF5 (*b*), BF6 (*c*), and BF7 (*d*)

The effect of CTAB

The effect of CTAB on $BaFe_{12}O_{19}$ particles in this method is examined by varying the amount of CTAB from 0 to 3.0 g, while the Fe/Ba ratio and ammonium carbonate are fixed at 11 and 4.0 g, respectively. Figure 2 shows the XRD patterns of BF4, BF5, BF6, and BF7 (Table 1). Clearly, all samples exhibit quite similar XRD patterns assigned to $BaFe_{12}O_{19}$ crystals, implying that CTAB are not necessary for forming $BaFe_{12}O_{19}$ phase. However, SEM images (Fig. 3) reveal the essential effect of CTAB, which plays a critical role in the morphology and particle size of $BaFe_{12}O_{19}$. In the absence of CTAB, the sample BF4 (Fig. 3a) shows very irregular particles, and no typically hexagonal platelet-like structure can be observed, which is mainly attributed to their incomplete crystallization at relative low-calcined temperature [41]. In the presence of CTAB, the typical platelet-like structure appears instead of irregular particles, especially in BF6 and BF7 (Fig. 3b–d), indicating that CTAB can effectively assemble the ferrite particles to produce regular hexagonal structure. More importantly, the platelet size of $BaFe_{12}O_{19}$ decreases reasonably with the increased amount of CTAB (Fig. 3c–d), demonstrating that CTAB is a favorable additive for reducing the particle size of $BaFe_{12}O_{19}$ in the solvent-free route.

Figure 4 shows the magnetic hysteresis loops of BF4, BF5, BF6, and BF7, and their corresponding parameters (H_c, M_s, M_r) are presented in Table 2. The sample BF4

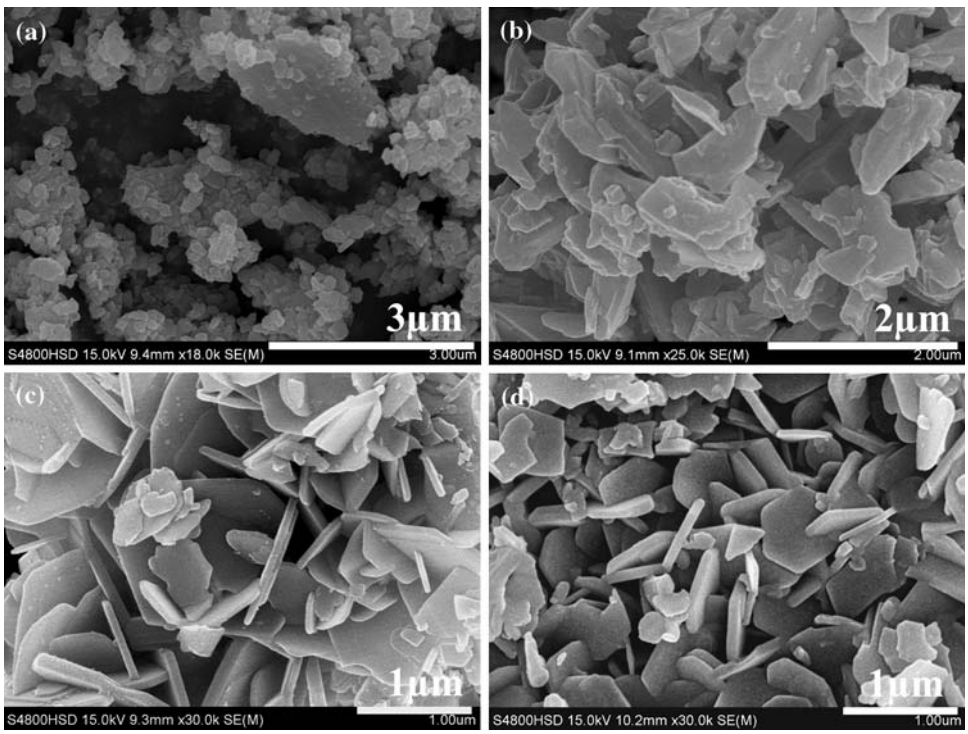

Fig. 3 SEM images of $BaFe_{12}O_{19}$ particles with different amount of CTAB. BF4 (**a**), BF5 (**b**), BF6 (**c**), and BF7 (**d**)

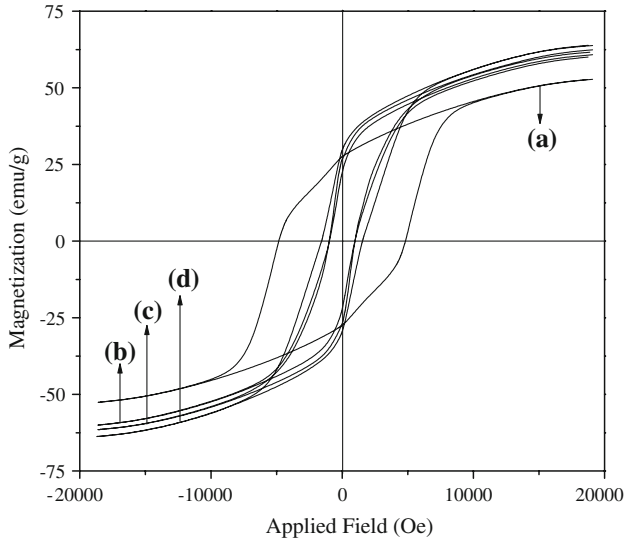

Fig. 4 Field-dependent magnetization curves of $BaFe_{12}O_{19}$ particles with different amount of CTAB. BF4 (*a*), BF5 (*b*), BF6 (*c*), and BF7 (*d*)

Table 2 Magnetic properties of prepared samples

Samples	M_r (emu/g)	M_s (emu/g)	H_c (Oe)	M_r/M_s
BF2	26.8	62.4	1018	0.43
BF4	27.5	52.8	4862	0.52
BF5	21.6	60.7	980	0.36
BF6	26.8	62.4	1018	0.43
BF7	30.6	63.9	1589	0.48
BF9	24.5	60.5	1060	0.41
BF10	26.8	62.4	1018	0.43
BF11	28.0	63.1	1014	0.44

BF2, BF6, and BF10 are identical sample

without CTAB exhibits very large intrinsic coercivity ($H_c = 4862$ Oe) and characteristics of single magnetic domains ($M_r/M_s = 0.52$) [42], the results imply that BF4 are composed of relatively small $BaFe_{12}O_{19}$ particles, it is in good agreement with that of SEM. However, it has to mention that the saturation magnetization of BF4 (52.8 emu/g) is too far away from the theoretically estimated value of 72 emu/g [43], further suggestive of deficiently crystalline $BaFe_{12}O_{19}$ particles in BF4 [41]. By comparison, in the presence of CTAB, the saturation magnetization of BF5, BF6, and BF7 are significantly enhanced (60.7–63.9 emu/g, Table 2), which are comparable with that of ever reported ultrafine barium ferrite powders by other chemical methods [24, 25, 39–41]. It is likely that the improvement in saturation magnetization can be attributed to more complete crystallization of the $BaFe_{12}O_{19}$ phase [41]. By considering that all samples (BF4–BF7) are prepared under the same conditions except CTAB amounts, it is believable that CTAB has special effect on promoting the crystallization of the $BaFe_{12}O_{19}$ particles, but the specific mechanism is not clear as yet. Previously, some groups always utilized the molten salt flux to promote the crystallinity of $BaFe_{12}O_{19}$ phase, then resulting in forming hexagonal particles with large saturation magnetization (>60 emu/g) at relatively low temperature (800–1000 °C) [44–46]. However, the obtained products should be repeatedly washed with vast water to remove the additive salts. In our case, CTAB seems to be comparably effective with the molten salt flux, but it is easier to remove by calcination.

Additionally, it is also found that BF5, BF6, and BF7 have low-intrinsic coercivity (980–1589 Oe, Table 2) due to their relatively big particle sizes (Fig. 3b–d). It is well known that the coercivity of barium ferrite depends on many factors, such as chemical composition, particle size, degree of crystallinity, microstructure, magnetic anisotropy, etc. However, recent progress indicates that the coercivity is strongly influenced by the particle size [47–54], whose variation can also induce the obvious change in saturation magnetization and magnetic anisotropy, etc. In our case, these samples (BF5–BF7) are synthesized under the same conditions (chemical composition, calcination temperature, calcination time, etc.); therefore, it is reliable that the relatively high coercivity of BF7 comes from its relatively small particle size. These results further confirm the effect of CTAB in decreasing the particle size, which are quite consistent of with the results of SEM. From further investigation on the value of M_r/M_s, we can observe that it increases gradually with the amount of CTAB (0.36–0.48, Table 2), especially BF7 with the maximum CTAB gives the value of M_r/M_s at 0.48, which is quite close to the theoretical value ($M_r/M_s \approx 0.5$) of single magnetic domains particles [42]. However, according to Stoner and Wohlfarth [55], the particle size below single-domain critical radius favor a higher coercivity (ca. 5,000 Oe) due to the pinning effects of more boundaries. Thus, BF5, BF6, and BF7 have essential characteristic of multiple magnetic domains.

The effect of ammonium carbonate

The effect of ammonium carbonate is also studied by varying the amount from 0 to 6.0 g, while the Fe/Ba ratio and CTAB are fixed at 11 and 2.0 g, respectively. Figure 5 shows the XRD patterns of BF8, BF9, BF10, and BF11 (Table 1). As can be observed, when there is no ammonium carbonate, the sample BF8 exhibits multispecies XRD patterns (Fig. 5a), and α-Fe_2O_3 is considered as the dominant phase rather than $BaFe_{12}O_{19}$. When ammonium carbonate is 2.0 g, the sample BF9 exhibits typical XRD

patterns of $BaFe_{12}O_{19}$, but there still exists a little α-Fe_2O_3 (Fig. 5b). Increasing ammonium carbonate to 4.0 or 6.0 g, the content of α-Fe_2O_3 is further decreased (Fig. 5c, d).

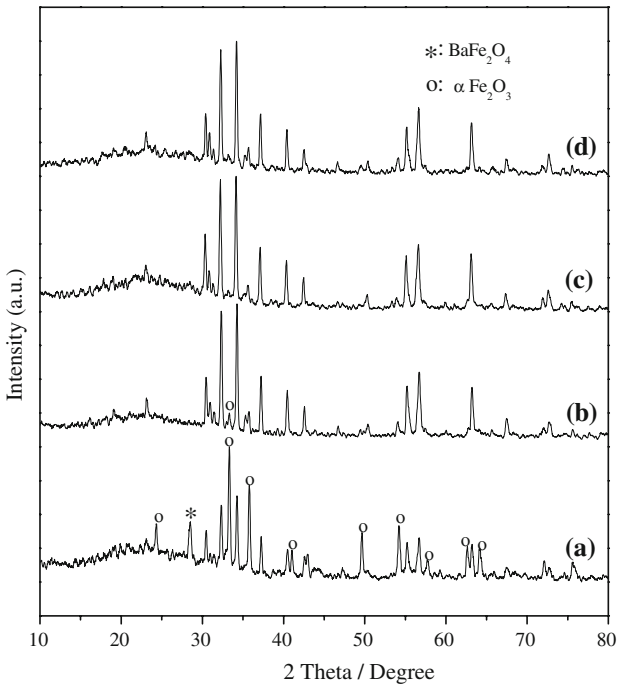

Fig. 5 XRD patterns of $BaFe_{12}O_{19}$ particles with different amount of ammonium carbonate. BF8 (*a*), BF9 (*b*), BF10 (*c*), and BF11 (*d*). The peaks marked with *circle* and *asterisk* are assigned to α-Fe_2O_3 and $BaFe_2O_4$, respectively

These results suggest that ammonium carbonate may be paramount for the formation of $BaFe_{12}O_{19}$ phase.

Figure 6 shows the SEM images of BF8, BF9, BF10, and BF11 (Table 1). In the absence of ammonium carbonate, the sample BF8 displays disordered particles with few platelets due to the presence of large amounts of α-Fe_2O_3 (Fig. 5a). In contrast, the sample BF9 shows obvious platelet-like structure, although they are agglomerate in some extent. In the presence of more ammonium carbonate, BF10 and BF11 exhibit typically hexagonal platelet-like particles with similar size. These phenomena indicate that ammonium carbonate can be helpful for formation and dispersion of hexagonal platelet-like $BaFe_{12}O_{19}$ particles, but less effective on particle size than CTAB, which can be further supported by the results of VSM (Fig. 7; Table 2). For instance, BF9 with 2.0 g of ammonium carbonate gives the saturation magnetization, intrinsic coercivity and M_r/M_s at 60.5 emu/g, 1060 Oe and 0.41, respectively. BF10 with 4.0 g of ammonium carbonate shows these values at 62.4 emu/g, 1018 Oe, and 0.43, while further increasing ammonium carbonate (BF11) leads to negligible variation in magnetic properties (63.1 emu/g, 1014 Oe and 0.44). As mentioned above [47–54], this phenomenon indicates that there is no obvious variation in particle size for BF9–BF11 by changing the amount of ammonium carbonate. Besides, the magnetic measurements of sample BF8 are not showed because the large amount of hematite present in this sample distorted the magnetic response.

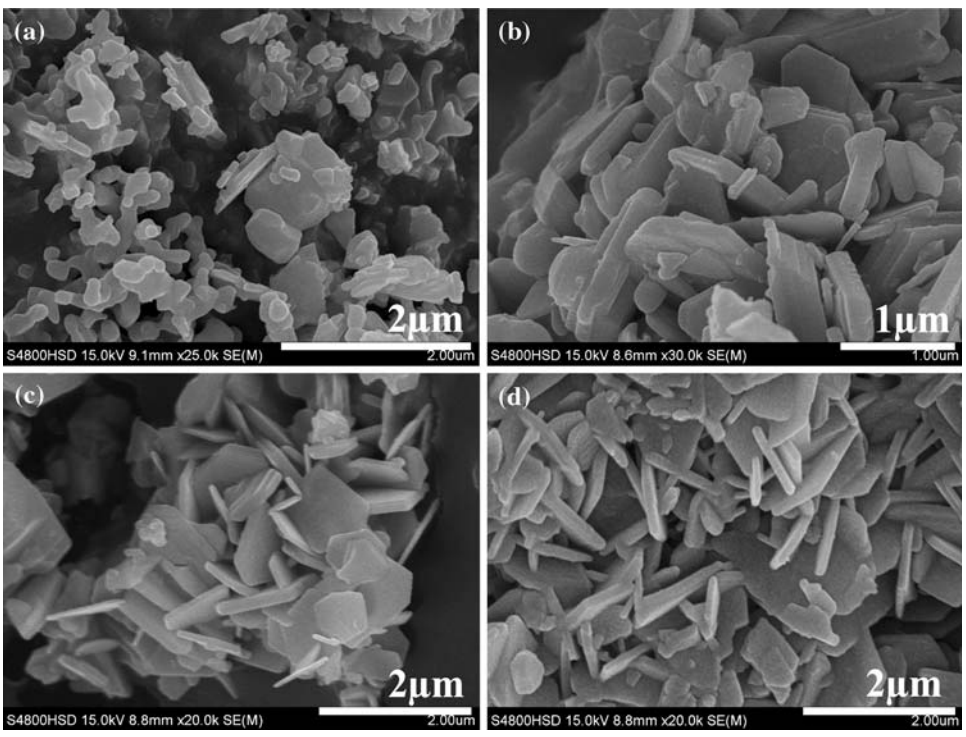

Fig. 6 SEM images of $BaFe_{12}O_{19}$ particles with different amount of ammonium carbonate. BF8 (**a**), BF9 (**b**), BF10 (**c**), and BF11 (**d**)

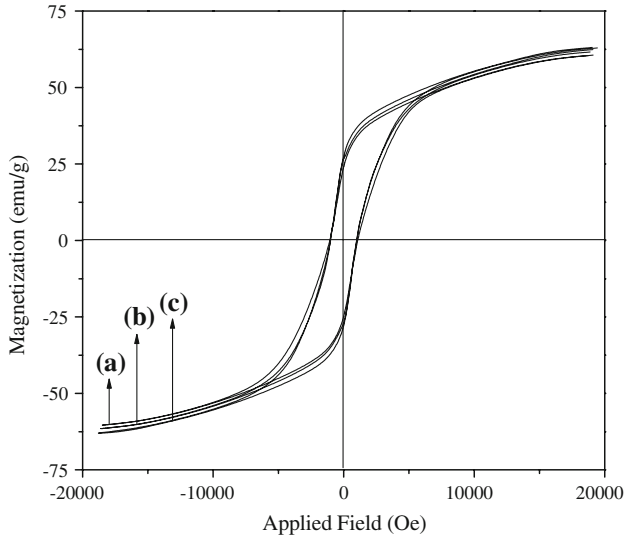

Fig. 7 Field-dependent magnetization curves of $BaFe_{12}O_{19}$ particles with different amount of ammonium carbonate. BF9 (*a*), BF10 (*b*), and BF11 (*c*)

Preparative method

It is well known that conventional ceramic method for barium ferrite ($BaFe_{12}O_{19}$) generally involves mechanical mixing, grinding, and calcination of the constituent oxides/carbonates, which is quite complex and time-consuming process. The major reason is the reacting species are molecular level mixture, they need long time and high temperature to migrate over large distances to produce well crystalline $BaFe_{12}O_{19}$ phase [56]. In some ways, our route is similar to conventional ceramic method except the presence of CTAB, just which acts as an excellent flux and makes our route superior to the conventional ceramic method, including shortened reaction time, typically hexagonal structure, small particle size, etc.

Recently, several facile and unconventional methods have also been applied to prepare fine $BaFe_{12}O_{19}$ particles, but solvent is absolutely necessary, so that there is always a large amount of waste alkaline solution. On the contrary, the preparation of $BaFe_{12}O_{19}$ is solvent-free in the current work, only involving simply calcination of mixed barium nitrate, ferric nitrate, CTAB, and ammonium carbonate without any unexpected reaction waste. Obviously, solvent-free synthesis of $BaFe_{12}O_{19}$ is an environmentally benign method, compared with those unconventional routes. More important, this facile and green route will stimulate the synthesis of other multiple oxides, actually, the synthesis of heteroatom-substituted barium ferrite, perovskite and spinel in this route are being carried out.

Conclusion

In summary, we have successfully synthesized hexagonal barium ferrite ($BaFe_{12}O_{19}$) through a facile method in the absence of any solvent. The obtained products exhibit well crystalline phase of $BaFe_{12}O_{19}$, typical platelet-like structure and large saturation magnetization, even submicrometer particle size under the optimum condition. Moreover, the characterization results indicate that the proper Fe/Ba ratio can suppress the intermediate phase such as α-Fe_2O_3 and $BaFe_2O_4$, CTAB can promote the crystallinity of $BaFe_{12}O_{19}$ and reduce the particle size, and ammonium carbonate is the key for forming $BaFe_{12}O_{19}$ phase. Very importantly, we do not think this method will be limited in the formation of $BaFe_{12}O_{19}$, it may open a door for preparation of a series of other functional materials.

Acknowledgements This work is supported by National Natural Science Foundation of China (20776032), China Postdoctoral Science Foundation (20090450979), Project Supported by Development Program for Outstanding Young Teachers in Harbin Institute of Technology (HITQNJS.2009.034) and Innovative Foundation of Heilongjiang Academy of Sciences (HKXY-CX-07001-03).

References

1. Kojima H (1982) In: Wohlfarth EP (ed) Ferromagnetic materials. North Holland, Amsterdam, chapter 5
2. Pillai V, Kumar P, Multani MS, Shah DO (1993) Colloid Surf A Physicochem Eng Asp 80:69
3. Liu X, Wang J, Gan LM, Ng SC (1999) J Magn Magn Mater 195:452
4. Yamamori K, Suzuki T, Fujiwara T (1986) IEEE Trans Magn 22:1188
5. Carreno TG, Morales MP, Serna CJ (2000) Mater Lett 43:97
6. Qiu JX, Gu MY (2006) J Alloys Compd 415:209
7. Xu P, Han XJ, Wang C, Zhao HT, Zhang WJ (2008) Mater Chem Phys 108:196
8. Ghasemi A, Hossienpour A, Morisako A, Saatchi A, Salehi M (2006) J Magn Magn Mater 302:429
9. Stablin H (1982) In: Wohlfarth EP (ed) Ferromagnetic materials. North Holland, Amsterdam, chapter 7
10. Haneda K, Miyakama C, Kojima H (1974) J Am Ceram Soc 57:354
11. Jacobo SE, Blesa MA, Domingo-Pascual C, Rodriguez-Clemente R (1997) J Mater Sci 32:1025. doi:10.1023/A:1018582423406
12. Lisjak D, Drofenik M (2007) J Mater Sci 42:8606. doi:10.1007/s10853-007-1850-0
13. Mishra D, Anand S, Panda RK, Das RP (2004) Mater Chem Phys 86:132
14. Drofenik M, Kristl M, Znidarsic A, Hanzel D, Lisjak D (2007) J Am Ceram Soc 90:2057
15. Yamauchi T, Tsukahara Y, Sakata T, Mori H, Chikata T, Katoh S, Wada Y (2009) J Magn Magn Mater 321:8
16. Topal U, Ozkan H, Sozeri H (2004) J Magn Magn Mater 284:416
17. Topal U, Ozkan H, Topal KG (2006) J Alloys Compd 422:276
18. Zhong W, Ding W, Zhang N, Hong J, Yan Q, Du Y (1997) J Magn Magn Mater 168:196
19. Fu YP, Lin CH, Pan KY (2004) J Alloys Compd 364:221
20. Mali A, Ataie A (2005) J Alloys Compd 399:245

21. Wang L, Zhang Q (2008) J Alloys Compd 454:210
22. Hovis DB, Faber KT, Kenik EA (2008) J Mater Sci 43:1836. doi: 10.1007/s10853-007-2375-2
23. Liu X, Wang J, Gan LM, Ng SC, Ding J (1998) J Magn Magn Mater 184:344
24. Xu P, Han X, Wang M (2007) J Phys Chem C 111:5866
25. Kubo O, Ido T, Yokoyama H (1982) IEEE Trans Magn 18:1122
26. Tang X, Zhao BY, Hu KA (2006) J Mater Sci 41:3867. doi: 10.1007/s10853-006-6676-7
27. Ye XR, Jia DZ, Yu JQ, Xin XQ, Xue Z (1999) Adv Mater 11:941
28. Hay JN, Raval HM (1998) J Mater Chem 8:1233
29. Liu XM, Lu GQ, Yan ZF (2004) J Phys Chem B 108:15523
30. Sun Y, Ma S, Du Y, Yuan L, Wang S, Yang J, Deng F, Xiao FS (2005) J Phys Chem B 109:2567
31. Ding Y, Shen X, Sithambaram S, Gomez S, Kumar R, Crisostomo VMB, Suib SL, Aindow M (2005) Chem Mater 17:5382
32. Lotnyk A, Graff A, Senz S, Zakharov ND, Hesse D (2008) Solid State Sci 10:702
33. Guo Q, Yang Q, Yi C, Zhu L, Xie Y (2005) Carbon 43:1386
34. Yue W, Zhou Z (2007) Chem Mater 19:2359
35. Joshi UA, Chung SH, Lee JS (2005) J Solid State Chem 178:755
36. Jung KS, Kwon JH, Shon SE, Ko JP, Shin JS, Park SS (2004) J Mater Sci 39:723. doi:10.1023/B:JMSC.0000011541.91490.88
37. Ataie A, Heshmati-Manesh S, Kazempour H (2002) J Mater Sci 37:2125. doi:10.1023/A:1015254221872
38. Pullar RC, Bhattacharya AK (2002) Mater Lett 57:537
39. Topal U, Ozkan H, Dorosinskii L (2007) J Alloys Compd 428:17
40. Huang J, Zhuang H, Li W (2003) Mater Res Bull 38:149
41. Mali A, Ataie A (2005) Scripta Mater 53:1065
42. Chikazumi S (1964) Physics of magnetism. Wiley, New York
43. Haneda K, Kojima H (1973) J Appl Phys 44:3760
44. Arendt RH, Rosolowski ZH, Szymaszek JW (1979) Mater Res Bull 14:703
45. Chin TS, Hsu SL, Deng MC (1993) J Magn Magn Mater 120:64
46. Kim SD, Kim JS (2006) J Magn Magn Mater 307:295
47. Rezlescu L, Rezlescu E, Popa PD, Rezlescu N (1999) J Magn Magn Mater 193:288
48. Dho J, Lee EK, Park JY, Hur NH (2005) J Magn Magn Mater 285:164
49. Ding J, Maurice D, Miao WF, McCormick RG, Street R (1995) J Magn Magn Mater 150:417
50. Hylton TL, Parker MA, Ullah M, Coffey KR, Umphress R, Howard JK (1994) J Appl Phys 75:5960
51. Lu YF, Song WD (2000) Appl Phys Lett 76:490
52. Ren P, Guan JG, Cheng XD (2006) Mater Chem Phys 98:90
53. Mendoza-Suárez G, Matutes-Aquino JA, Escalante-García JI, Mancha-Molinar H, Ríos-Jara D, Johal KK (2001) J Magn Magn Mater 223:55
54. Janasi SR, Emura M, Landgraf FJG, Rodrigues D (2002) J Magn Magn Mater 238:168
55. Stoner EC, Wohlfarth EP (1948) Philos Trans Roy Soc Lond 240:599
56. Sankaranarayanan VK, Khan DC (1996) J Magn Magn Mater 153:337